Supplementary information for

Metal-Organic Frameworks built from a carborane linker isolating ideal one-dimensional large-spin chains of Co (S=3/2) or Ni (S=1)

Xiao-Bao Li,[1] Mark E. Light,[2] Ana Arauzo,[3] Elena Bartolomé, [1] José Giner Planas[1]**

[1] *Institut de Ciència de Materials de Barcelona (ICMAB-CSIC), Campus UAB, 08193 Bellaterra, Spain.*
[2] *School of Chemistry & Chemical Engineering, University of Southampton, Highfield, Southampton SO17 1BJ, UK.*
[3] *Instituto de Nanociencia y Materiales de Aragón (INMA), Departamento de Física de la Materia Condensada, CSIC-Universidad de Zaragoza, Zaragoza 50009, Spain.*

[*]Emails: jginerplanas@icmab.es, ebartolome@icmab.es

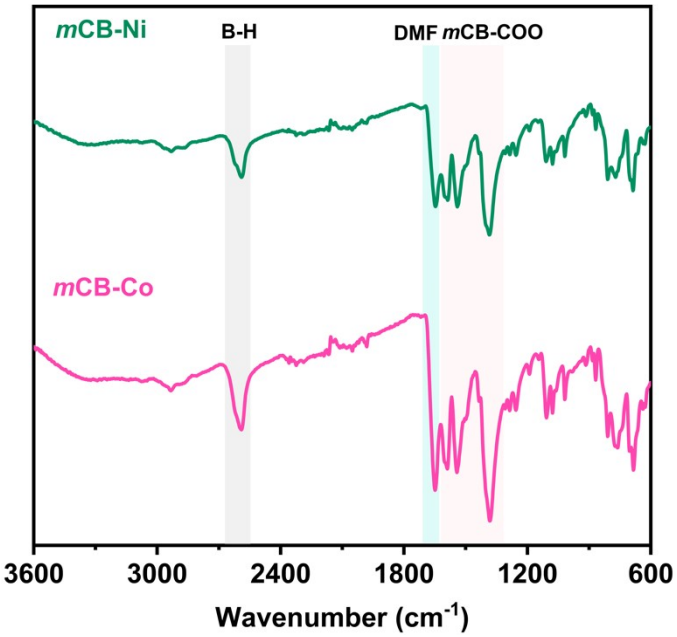

Fig. S1. FTIR spectra for ***m*CB-Co** and ***m*CB-Ni**. Bands for B-H (highlighted in dray) appear in the range 2590-2592 cm^{-1}, those highlighted in blue are attributed to C=O of DMF (1650 cm^{-1}) and those in the pink area (1587-1383 cm^{-1}) are attributed to O-C=O of *m*CBL linker.

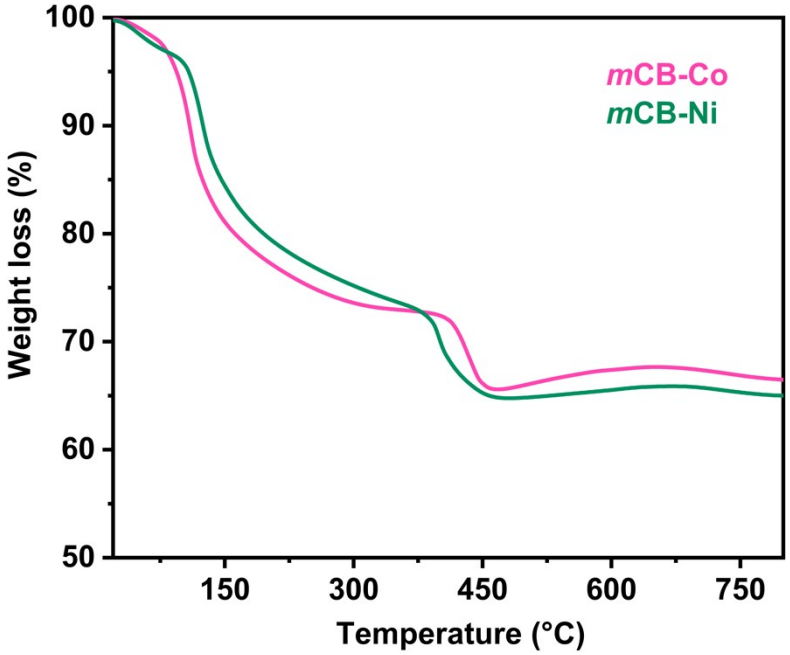

Fig. S2. Comparison of the TGA for ***m*CB-Co** and ***m*CB-Ni**.

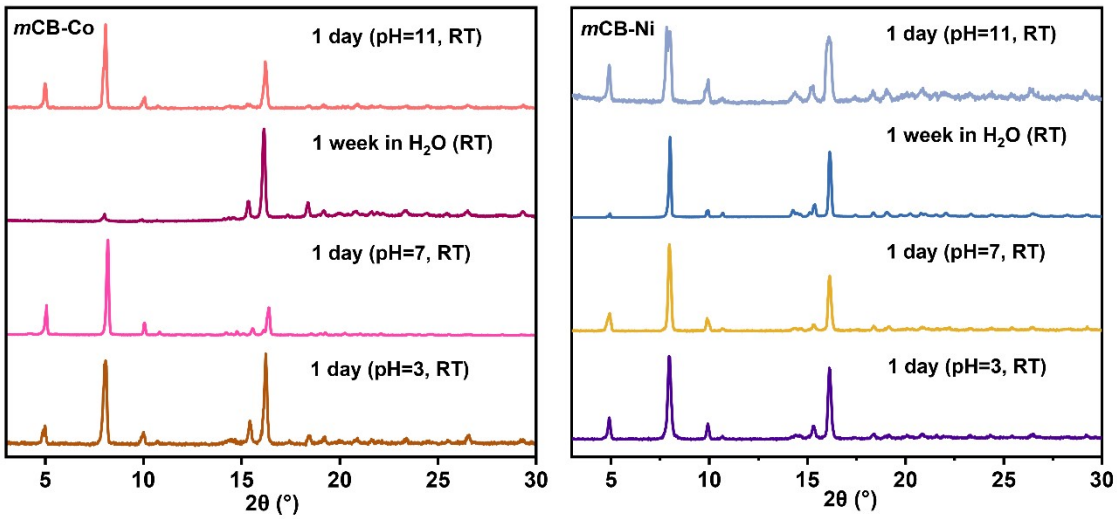

Fig. S3. Comparison of PXRD of ***m*CB-Co** and ***m*CB-Ni** after being 1 week in H_2O or 1 day in water solutions of various pH values.

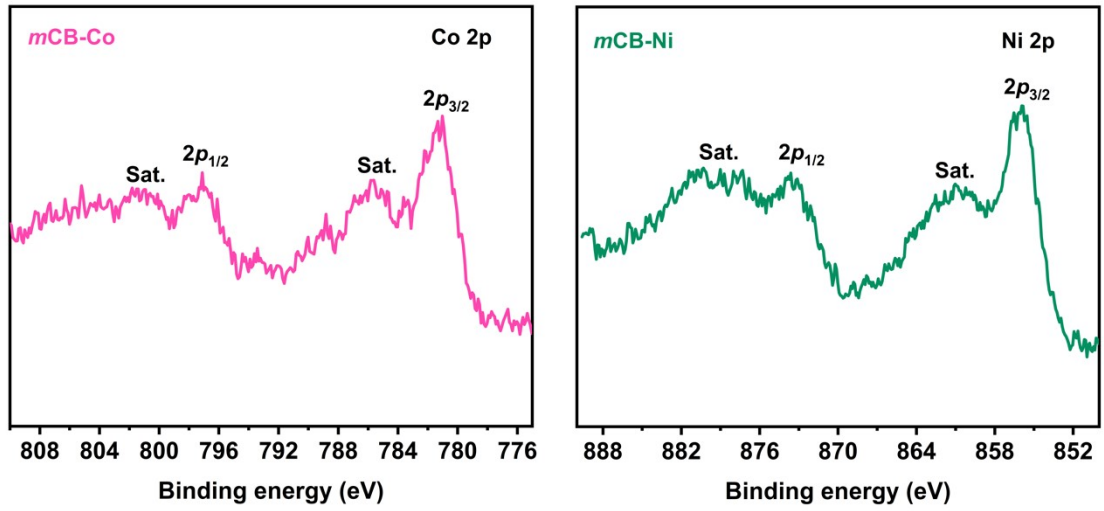

Fig. S4. Comparison of metal $2p_{1/2}$ and $2p_{3/2}$ peaks in the high resolution XPS spectra for ***m*CB-Co** and ***m*CB-Ni**.

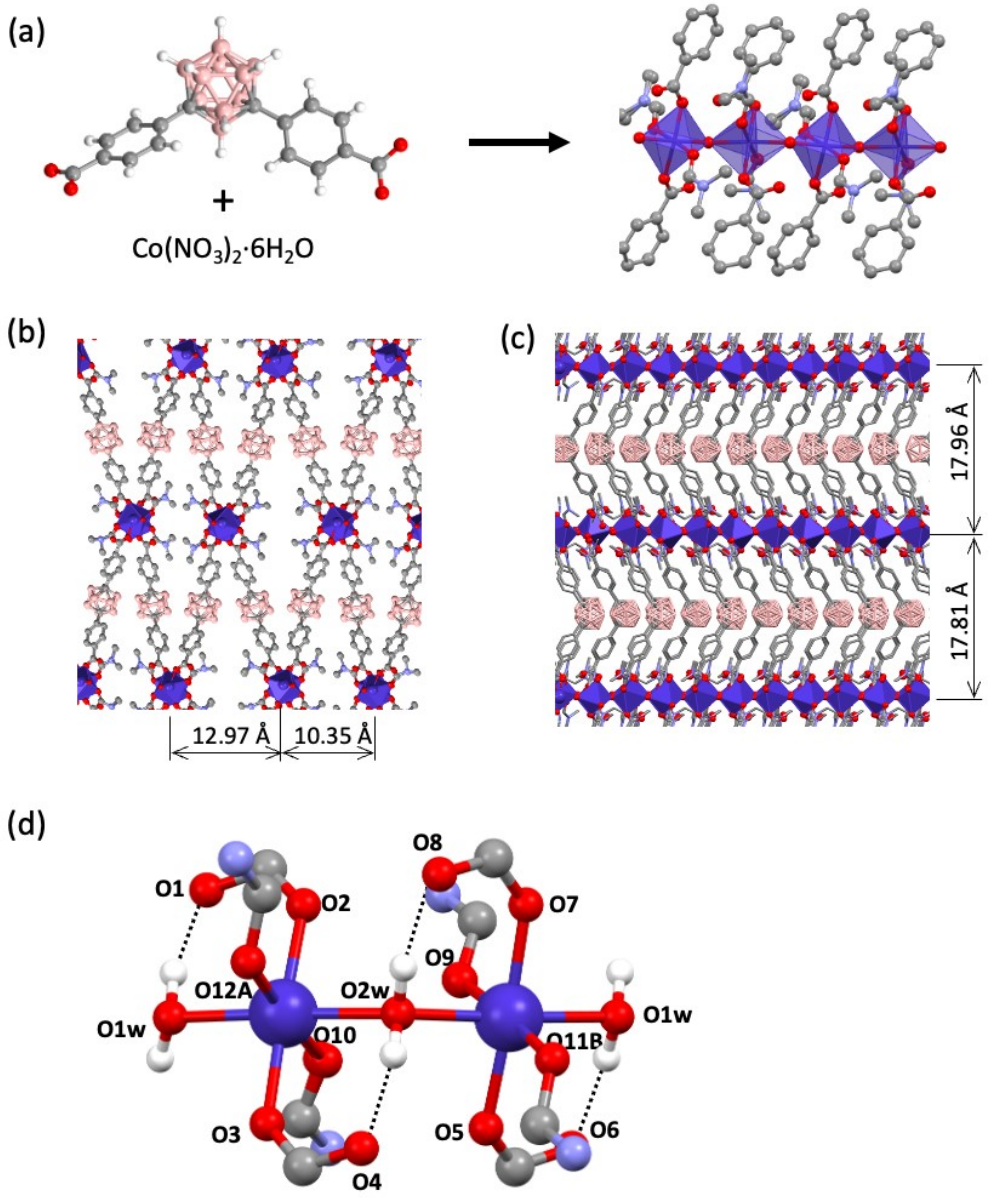

Fig. S5 Crystal structure of *m*CB-Co. (a) View of the coordination of *m*CB-L1 to the Co atoms showing the inorganic rod-shaped chains and (b, c) two perpendicular views of the extended 3D structure along the *b* and *a* axes, respectively. (d) Coordination environment of the Co^{II} atoms, including intramolecular OH···O hydrogen bonds (**O1w–H···O1:** H···O 1.83 Å, O···O 2.693(3) Å, OHO 161.6; **O2w–H···O4:** H···O 1.76 Å, O···O 2.654(3) Å, OHO 163.9; **O2w–H···O8:** H···O 1.78 Å, O···O 2.661(4) Å, OHO 161.7; **O1w–H···O6:** H···O 1.82 Å, O···O 2.695(4) Å, OHO 162.3). Parts of the ligands are omitted for clarity. Blue polyhedra represent the Co coordination spheres and H atoms are omitted for clarity. Color code: Co, dark blue; O, red; C, gray; N, blue; B, pink.

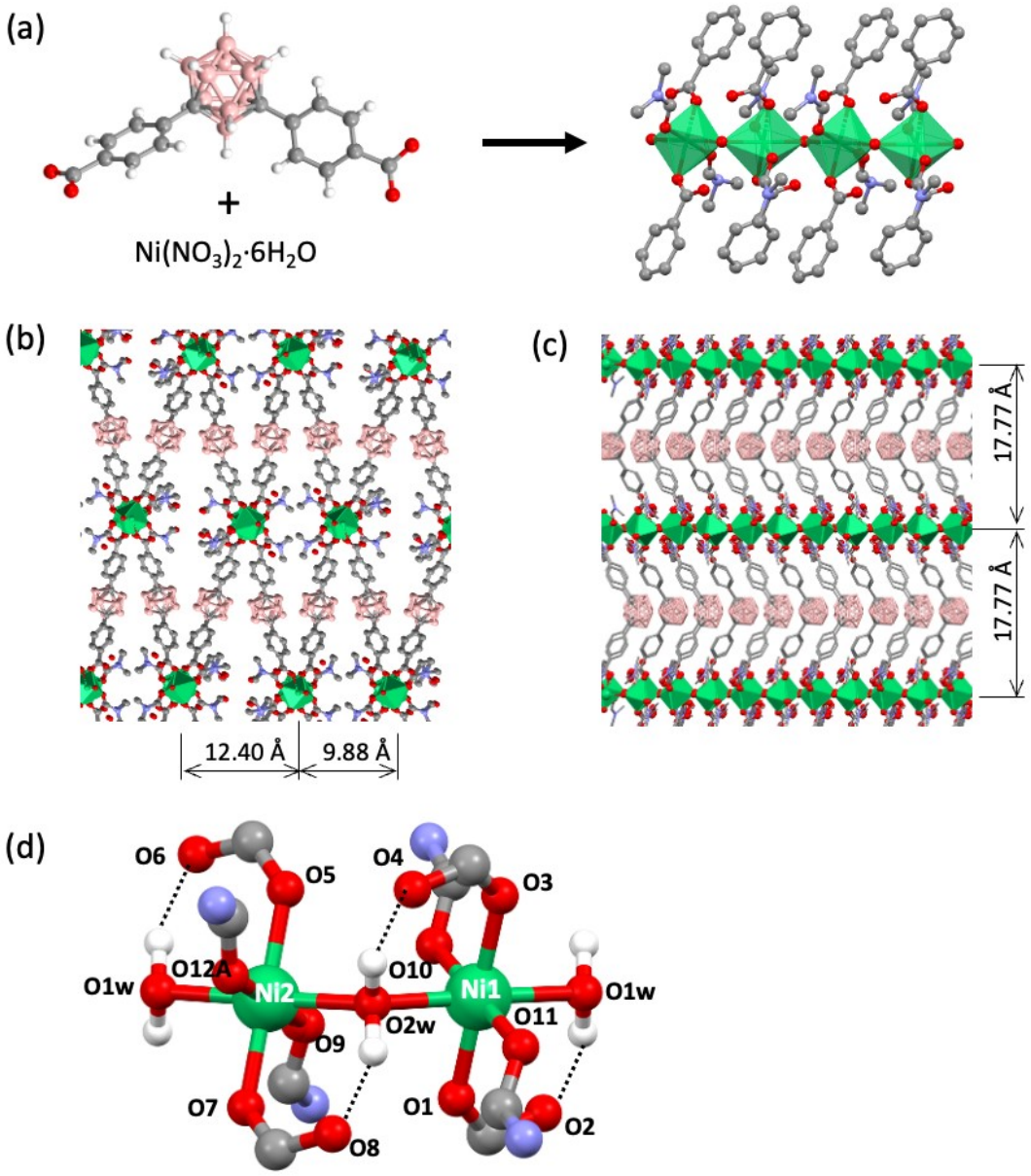

Fig. S6. Crystal structure of *m*CB-Ni. (a) View of the coordination of *m*CB-L1 to the Ni atoms showing the inorganic rod-shaped chains and (b, c) two perpendicular views of the extended 3D structure along the *b* and *a* axes, respectively. (d) Coordination environment of the Ni^{II} atoms, including intramolecular OH···O hydrogen bonds (**O1w–H···O2:** H···O 1.75 Å, O···O 2.663(3) Å, OHO 152.6; **O1w–H···O6:** H···O 1.75 Å, O···O 2.668(4) Å, OHO 152.2; **O2w–H···O4:** H···O 1.70 Å, O···O 2.616(3) Å, OHO 152.7; **O2w–H···O8:** H···O 1.71 Å, O···O 2.632(3) Å, OHO 152.6. Parts of the ligands are omitted for clarity. Green polyhedra represent the Ni coordination spheres and H atoms are omitted for clarity. Color code: Ni, green; O, red; C, gray; N, blue; B, pink.

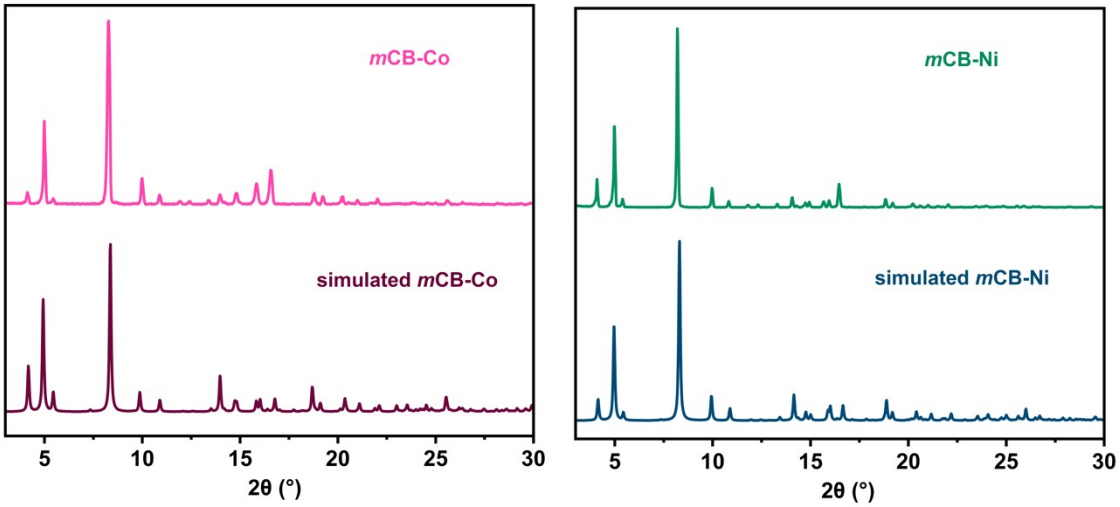

Fig. S7. Experimental and calculated PXRD patterns for ***m*CB-Co** and ***m*CB-Ni**.

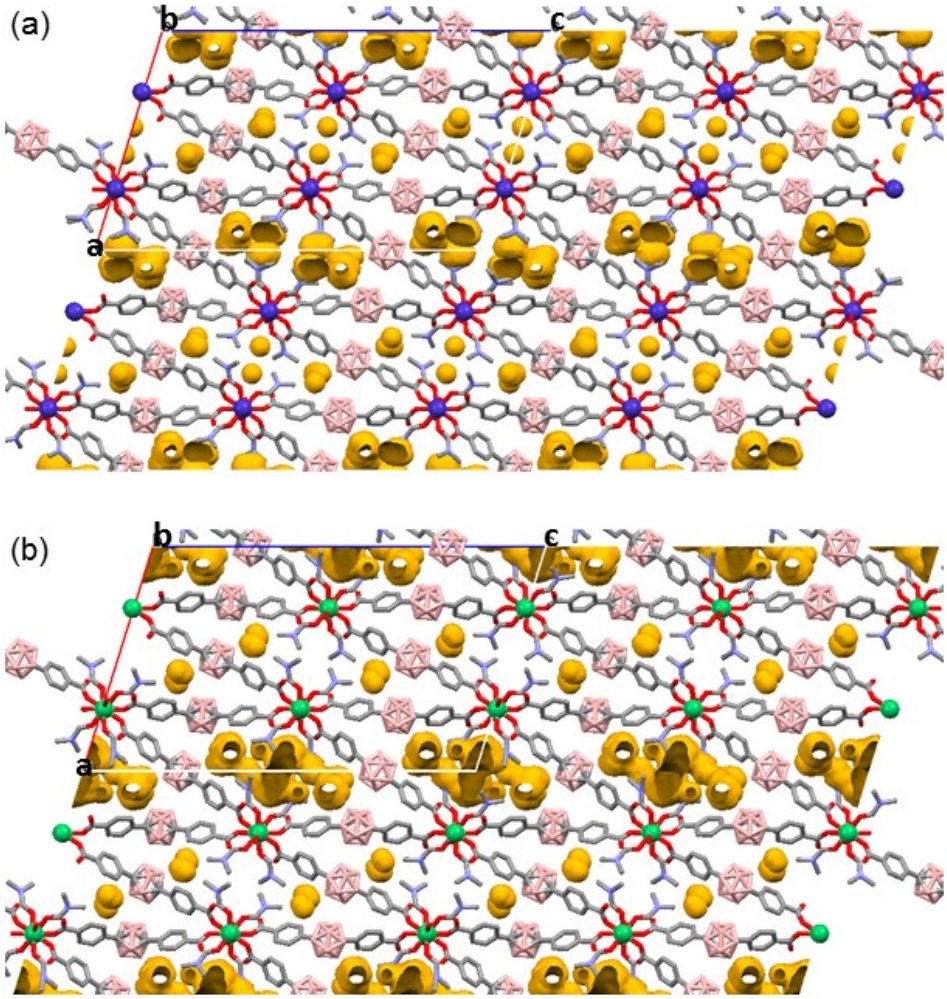

Fig. S8. Voids for ***m*CB-Co** (a) and ***m*CB-Ni** (a) along the *b* axis, determined by Mercury measured with a probe radius of 1.0 Å.[1] The calculated void values are 6.0 % of the unit cell (362.78 Å^3) for ***m*CB-Co** and 8.4 % of the unit cell (501.19 Å^3) for ***m*CB-Ni**.

Table S1. Crystal and Structure Refinement data for ***m*CB-Co** and ***m*CB-Ni**.

	***m*CB-Co**	***m*CB-Ni**
Formula	$C_{44}H_{68}B_{20}Co_2N_4O_{14}$	$C_{41.45}H_{66.25}B_{20}N_{3.15}Ni_2O_{15.35}$
F.W.	1211.08	1187.94
Temperature	100(2) K	99.99(10) K
Space group	*P*2/*c*	*P*2/*c*
a (Å)	22.08450(10)	22.2725(2)
b (Å)	7.71750(10)	7.54680(10)
c (Å)	37.4206(2)	37.2343(4)
α (deg)/°	90.00	90.00
β (deg)/°	107.0650(10)	107.3850(10)
γ (deg)/°	90.00	90.00
V (Å^3)	6097.06(10)	5972.67(12)
Z	4	4
ρ_{calc} (g/cm^3)	1.319	1.321
μ (mm^{-1})	4.762	1.295
GOF on F^2	1.035	1.033
R_1,wR_2[I>2σ (I)][a]	0.0755, 0.2258	0.0758, 0.2231
R_1, wR_2 (all data)	0.0784, 0.2288	0.0895, 0.2366
CCDC Codes	2267757	2341767

[a] $R_1 = \sum||F_o| - |F_c||/\sum|F_o|$, [b] $wR_2 = \{\sum w[(F_o)^2 - (F_c)^2]^2/\sum w[(F_o)^2]^2\}^{1/2}$

Table S2. Selected bond distances (Å) for ***m*CB-Co** and ***m*CB-Ni**.

		***m*CB-Co**	
Co(1)–O(1W)	2.169(3)	Co(2)–O(1W)	2.167(3)
Co(1)–O(2W)	2.134(3)	Co(2)–O(2W)	2.136(3)
Co(1)–O(2)	2.013(2)	Co(2)–O(5)	2.007(2)
Co(1)–O(3)	2.037(2)	Co(2)–O(7)	2.034(2)
Co(1)–O(10)(DMF)	2.099(3)	Co(2)–O(9)(DMF)	2.105(3)
Co(1)–O(12A)(DMF)	2.14(1)	Co(2)–O(11A)(DMF)	2.137(9)
Co(1)–O(12B)(DMF)	2.16(2)	Co(2)–O(11B)(DMF)	2.177(7)
		***m*CB-Ni**	
Ni(1)–O(1W)	2.100(3)	Ni(2)–O(1W)	2.096(3)
Ni(1)–O(2W)	2.090(3)	Ni(2)–O(2W)	2.084(3)
Ni(1)–O(1)	1.989(3)	Ni(2)–O(5)	1.989(3)
Ni(1)–O(3)	2.006(2)	Ni(2)–O(7)	2.001(3)
Ni(1)–O(10)	2.04(2)	Ni(2)–O(3W)	2.01
Ni(1)–O(11)	2.073(3)	Ni(2)–O(9)	2.103(5)
Ni(1)–O(5W)	2.04(2)	Ni(2)–O(12A)	2.072(5)

Magnetostructural correlation

Table S3. Summary of selected compounds previously reported that include 1D Co or Ni chains.

Compound	Dimension		M···M[a]	M–OH_2–M[b]	g[c]	J/k_B (K)[d]	J'/k_B (K)[e]	J'/J	T_N (K)[f]	Δ/k_B(K),[g] Δ_ξ/k_B(K)[h]	Ref.
	Structural	Magnetic									
	Co^{II} (S = 3/2)										
$[Co_2(m$CB-L$)_2(\mu_2$-$H_2O)_2(DMF)_4]_n$·solv	3D	1D	3.860	127.5	2.47	-4.65	-2.2x10^{-3}	4.7x10^{-4}	< 0.4	-	This work
$[Co_2(L)_2(\mu_2$-$H_2O)_2$ $(DMF)_4]_n$[i]	3D	1D	4.199	139.0	2.86	33.22	-	-	< 2	21.65, 6.44	2
Co(ox)(en)	1D	1D	-	-	2.5	-16.98	-	-	-	-	3
Co(ox)(en).2H_2O	1D	1D	-	-	2.6	-14.82	-	-	-	-	3
$[Co(ox)(Htr)_2].2H_2O\}_n$	1D	1D	-	-	2.64	-13.38	-	-	-	-	4
$\{[Co(ox)(H_2O)_2]2H_2O\}_n$	1D	1D	-	-	2.51	-23.60	-	-	-	-	5
$[Co(m$-H2tpta$)(\mu_2$-$H_2O)(H_2O)_2]_n$	1D	1D	3.910	130.6	2.41	- 14.3	-	-	-	-	6
$\{[Co(H_2O)_2(L)_2].2H_2O\}_n$ L = 9-anthracenecarboxilato	1D	1D	-	-	-	-	-	-	-	8.11, 4.20	7
$\{[Co(H_2O)_2(L')_2].2H_2O\}_n$ L' = 4-quinolinecaroxylato	1D	1D	-	-	-	-	-	-	~0.6	4.80, 4.49	7
	Ni^{II} (S = 1)										
$[Ni_2(m$CB-L$)_2(\mu_2$-$H_2O)_2(DMF)_4]_n$·solv	3D	1D	3.774	128.8	2.21	-23.36	-8.6x10^{-4}	3.7x10^{-5}	< 0.3	-	This work
$[NiL_2$-$(\mu$-$N_3)]_n(ClO_4)_n]$	1D	1D	-	-	2.20	-22.2	-	-	-	-	8
$\{[Ni_2(p$-tpta$)(\mu_2$-$H_2O)_2(H_2O)_4]\cdot 2H_2O\}$	3D	1D	3.870	133.3	2.19	-45.05	-	-	-	-	6
$C_6H_5CH_2CH_2NH_3NiCl_3$	perovskite	1D	-	-	2.25	-25.5	-	-	10	-	9
$MANiCl_3$	perovskite	1D	-	-	2.271	-21.46	-	-	1.1	-	10
Y_2BaNiO_5	perovskite	1D	-	-	-	-285	-	< 10^{-2}	< 1.8	-	11

[a] Metal-to-metal distances (Å). [b] Metal-water-Metal angles (deg). [c] Gyromagnetic value. [d-e] Intrachain (J) and interchain (J') coupling (expressed in $H = -JS_iS_{i+1}$ Hamiltonian). [f] Magnetic long-range order transition temperature (T_N). [g-h] For SCMs, the energy barrier (Δ) for the magnetization reversal consists of the anisotropic energy Δ_A of the building unit of the chain and the correlation energy Δ_ξ for the interaction between the building units of the chain. [i] LH_2 = 3,30-(1,3,6,8-tetraoxobenzol[lmn][3,8]-phenanthroline-2,7(1H,3H,6H,8H)diyl)-di-benzoic acid. (ox = oxalate dianion; Htr = 1,2,4-triazole).

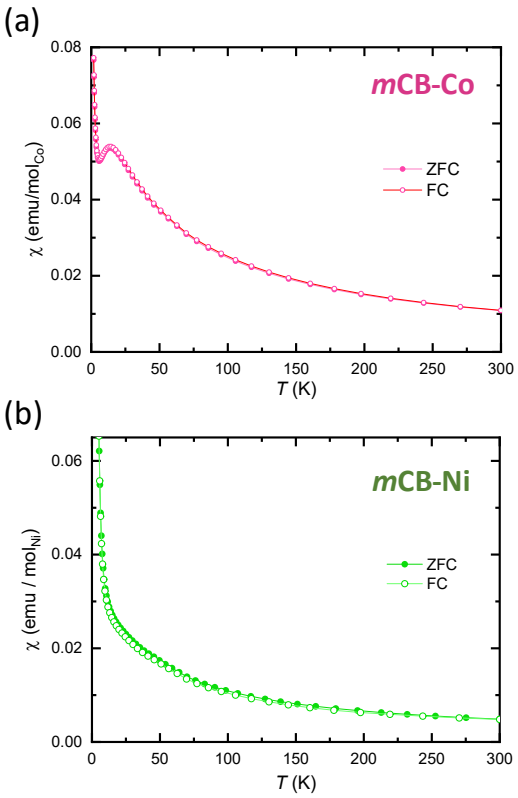

Fig. S9. Temperature-dependence of the magnetic susceptibility, χ(T), measured after a zero-field-cool (ZFC) and field-cool (FC) process, 0.02 T, for ***m*CB-Co** (a) and ***m*CB-Ni** (b).

Band Gaps Analysis

We have followed the recommendations from Andrade and coworkers for estimating the band gaps or our materials.[12] It follows a summary of E_g values (Table S4) and the plots (Figs S9-S10). As it can be seen in the plots, a more linear region is found in the direct plots than in the indirect ones. This seems to indicate the direct nature of our materials as semiconductors. This is further support by the fact that E_g (F(R)) values are closer to the direct $(F(R)^2$, $F(R)h\nu)^2$ and $(\alpha h\nu)^2)$ values.[12,13]

To estimate the band gap values, we fitted the linear portion of the curves to a line equation y = a + bx. By setting y=0, we calculated the points at which the line crosses the x-axis, corresponding to the band gaps. Errors correspond to values obtained from various fitted lines.

Table S4. Band gap values (E_g, eV) estimated through the plot of F(R), $F(R)^2$, $F(R)^{1/2}$, $(F(R)h\nu)^2$, $(Ah\nu)^2$, $(F(R)h\nu)^{1/2}$ or $(Ah\nu)^{1/2}$ versus the photon energy hν for ***m*CB-Co** and ***m*CB-Ni**.

Plot Method	***m*CB-Co**	$\lvert \Delta E_g$ ***vs*** **F(R)** $\rvert$	***m*CB-Ni**	$\lvert \Delta E_g$ ***vs*** **F(R)** $\rvert$
F(R)	3.66	0	4.09	0
Direct $(F(R)^2)$	3.83±0.02	0.17	4.20±0.01	0.11
Indirect $(F(R)^{1/2})$	3.43	0.23	3.50	0.59
Tauc direct $((F(R)h\nu)^2)$	3.88±0.03	0.22	4.20±0.02	0.11
Tauc indirect $((F(R)h\nu)^{1/2})$	3.43	0.23	3.54	0.55
Direct $(Ah\nu)^2$	3.68±0.01	0.02	4.08±0.02	0.01
Indirect $((Ah\nu)^{1/2})$	3.03	0.63	3.16	0.93

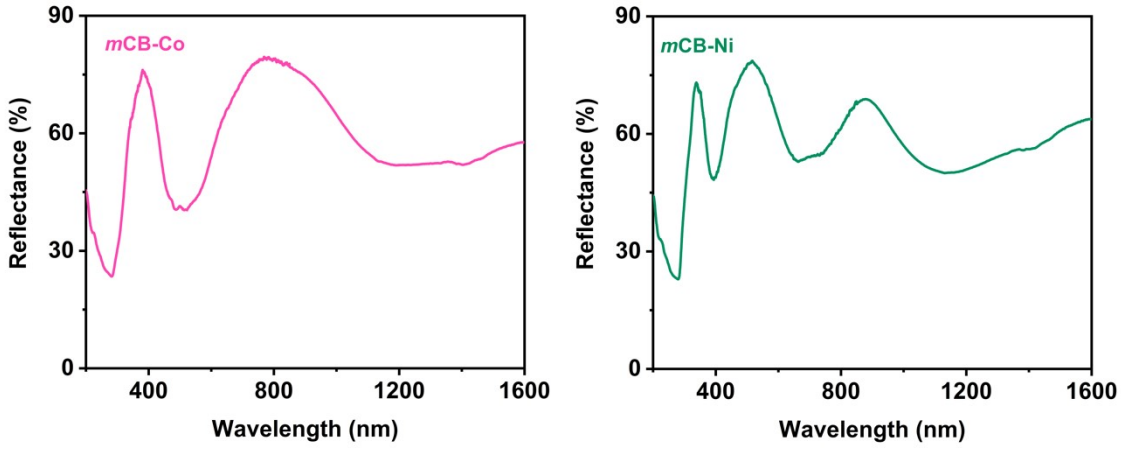

Fig. S10. UV-vis diffuse reflectance spectra of ***m*CB-Co** and ***m*CB-Ni**.

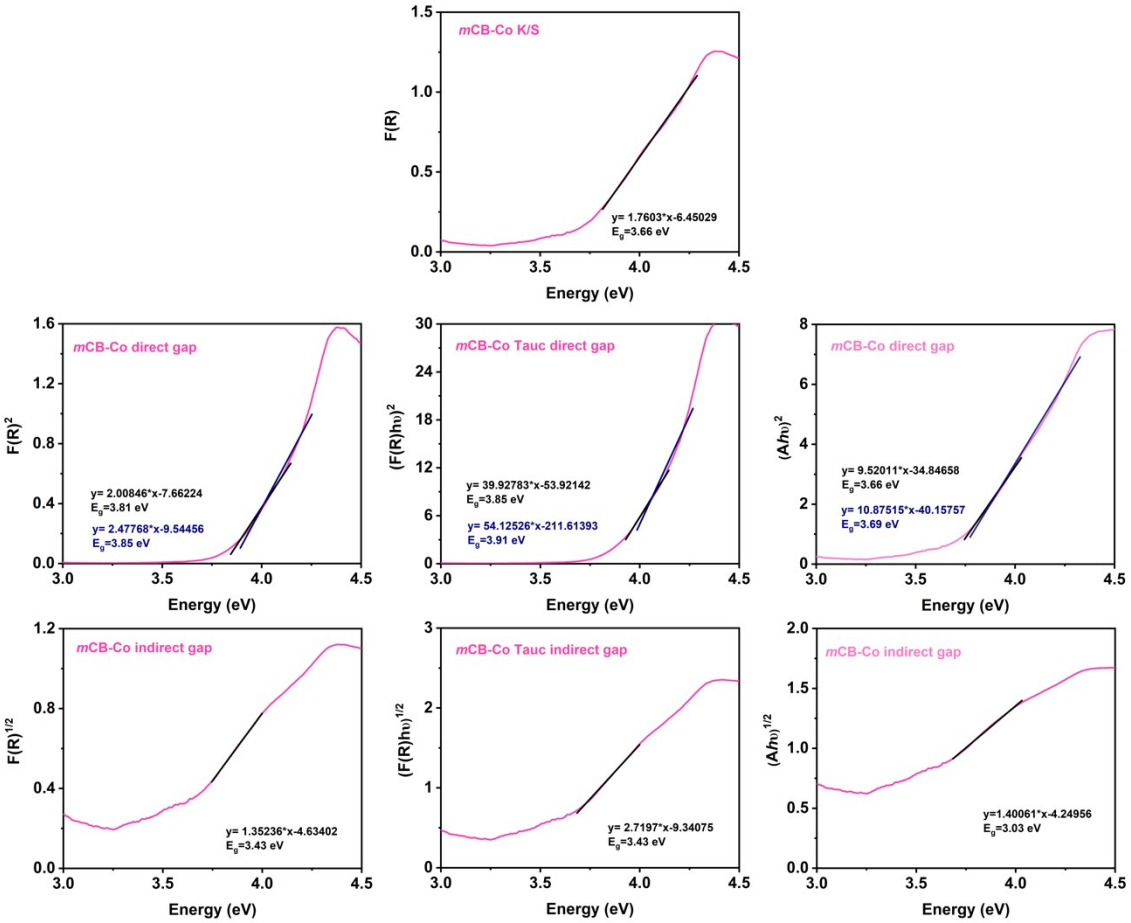

Figs. S11. Plots of F(R), $F(R)^2$, $F(R)^{1/2}$, $(F(R)h\nu)^2$, $(Ah\nu)^2$, $(F(R)h\nu)^{1/2}$ and $(Ah\nu)^{1/2}$ versus the photon energy hν for ***m*CB-Co**. Several fitted lines were created for the direct methods graphs to obtain the errors.

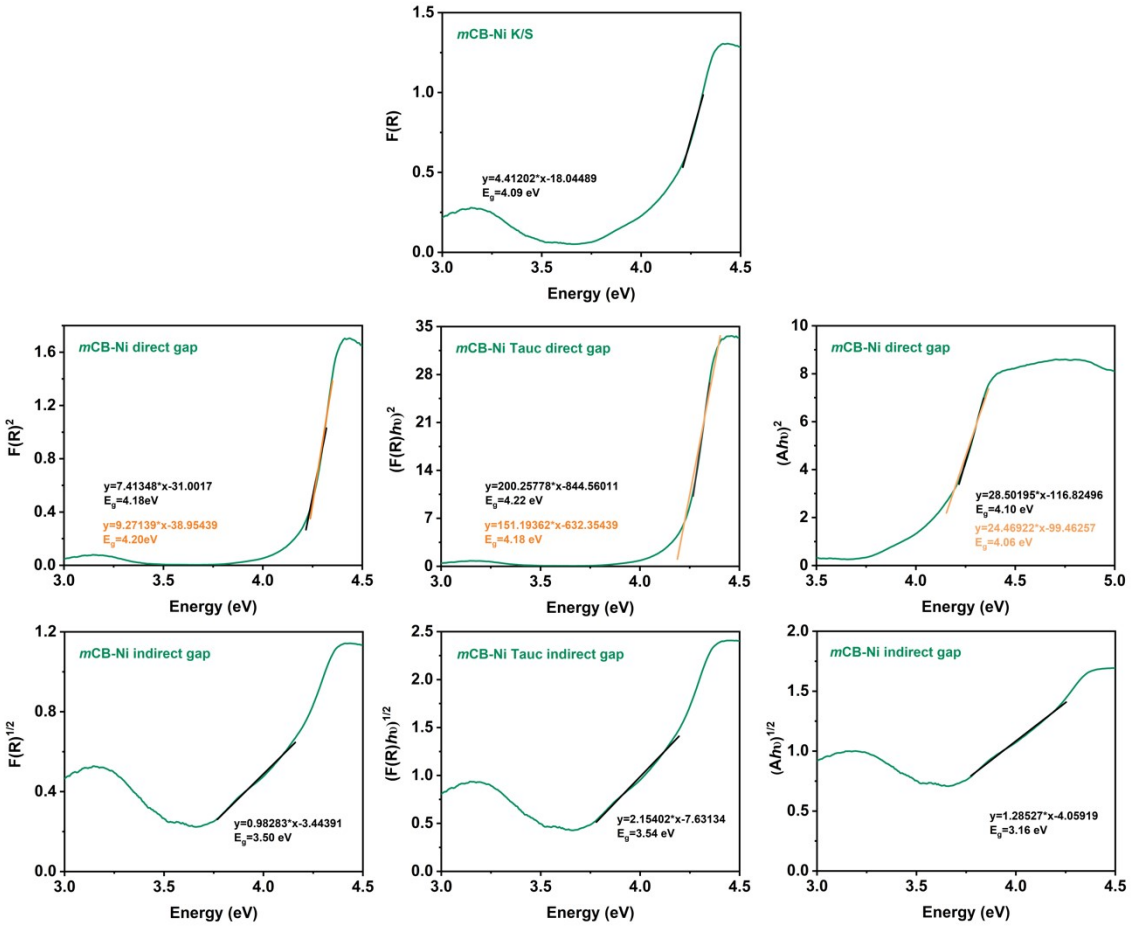

Figs. S12. Plots of F(R), $F(R)^2$, $F(R)^{1/2}$, $(F(R)h\nu)^2$, $(Ah\nu)^2$, $(F(R)h\nu)^{1/2}$ and $(Ah\nu)^{1/2}$ versus the photon energy hν for ***m*CB-Ni**. Several fitted lines were created for the direct methods graphs to obtain the errors.

References

1 C. F. MacRae, I. Sovago, S. J. Cottrell, P. T. A. Galek, P. McCabe, E. Pidcock, M. Platings, G. P. Shields, J. S. Stevens, M. Towler and P. A. Wood, *J Appl Crystallogr*, 2020, **53**, 226–235.

2 X. Ma, Z. Zhang, W. Shi, L. Li, J. Zou and P. Cheng, *ChemComm*, 2014, **50**, 6340–6342.

3 J. Kang, Y. Lee, S. Kim, H. Yun and J. Do, *Bull Korean Chem Soc*, 2014, **35**, 3244–3248.

4 D. Olea, U. García-Couceiro, O. Castillo, J. Gómez-Herrero and F. Zamora, *Inorganica Chim Acta*, 2007, **360**, 48–54.

5 U. García-Couceiro, O. Castillo, A. Luque, G. Beobide and P. Román, *Inorganica Chim Acta*, 2004, **357**, 339–344.

6 S. Feng, L. Shao‐Dong, H. Chun, W. Lin‐Tao and W. Zhi‐Jun, *Chinese Journal of Inorganic Chemistry*, 2022, **38**, 1421–1432.

7 Y. Zhang, Z.-Y. Liu, H.-M. Tang, B. Ding, Z.-Y. Liu, X.-G. Wang, X.-J. Zhao and E.-C. Yang, *Inorg Chem Front*, 2022, **9**, 5039–5047.

8 J. Ribas, M. Monfort, C. Diaz, C. Bastos, C. Mer and X. Solans, *Inorg.Chem.*, 1995, **34**, 4986–4990.

9 F. Lipps, A. H. Arkenbout, A. Polyakov, M. Günther, T. Salikhov, E. Vavilova, H.-H. Klauss, B. Büchner, T. M. Palstra and V. Kataev, *Low Temperature Physics*, 2017, **43**, 1298–1304.

10 T. Lee, D. B. Straus, K. P. Devlin, X. Gui, P. Louka, W. Xie and R. J. Cava, *Inorg Chem*, 2022, **61**, 10486–10492.

11 J. Darriet and L. P. Regnault, *Solid State Commun*, 1993, **86**, 409–412.

12 P. H. M. Andrade, C. Volkringer, T. Loiseau, A. Tejeda, M. Hureau and A. Moissette, *Appl Mater Today*, 2024, **37**, 102094.

13 P. H. M. Andrade, A. L. M. Gomes, H. G. Palhares, C. Volkringer, A. Moissette, H. F. V. Victória, N. M. A. Hatem, K. Krambrock, M. Houmard and E. H. M. Nunes, *J Mater Sci*, 2022, **57**, 4481–4503.